02

Controlled-aperture wave-equation migration

Lianjie Huang, Hongchuan Sun, and Michael C. Fehler, Los Alamos National Laboratory; Zhiming Li, Parallel Data Systems, Inc.*

Summary

We present a controlled-aperture wave-equation migration method that not only can reduce migration artifacts due to limited recording apertures and determine image weights to balance the effects of limited-aperture illumination, but also can improve the migration accuracy by reducing the slowness perturbations within the controlled migration regions. The method consists of two steps: migration aperture scan and controlled-aperture migration. Migration apertures for a sparse distribution of shots are determined using wave-equation migration, and those for the other shots are obtained by interpolation. During the final controlled-aperture migration step, we can select a reference slowness in controlled regions of the slowness model to reduce slowness perturbations, and consequently increase the accuracy of wave-equation migration methods that make use of reference slownesses. In addition, the computation in the space domain during wavefield downward continuation is needed to be conducted only within the controlled apertures and therefore, the computational cost of controlled-aperture migration step (without including migration aperture scan) is less than the corresponding uncontrolled-aperture migration. Finally, we can use the efficient split-step Fourier approach for migration-aperture scan, then use other, more accurate though more expensive, wave-equation migration methods to perform the final controlled-aperture migration to produce the most accurate image.

Introduction

Limited recording aperture used in real data acquisition requires that migration also be performed in a controlled aperture to obtain the most reliable image. The least-squares Kirchhoff migration (Nemeth et al., 1999) or limited-aperture Kirchhoff migration (Sun, 2000) can reduce migration artifacts due to limited recording aperture. It is important for amplitude-preserving migration to take the effects of limited-aperture illumination into account to obtain a reliable migration image. Controlled-aperture migration can be used to determine image weights to balance the effects of limited-aperture illumination in amplitude-preserving migration. Most studies on controlled-aperture migration have been concentrated on Kirchhoff migration.

For complex-structure imaging problems, wave-equation migration has the potential to produce more accurate images than Kirchhoff migration (Fehler and Huang, 2002). In this paper, we will present a controlled-aperture wave-equation migration method. It consists of two steps: (1) migration aperture scan using a wave-equation migration scheme, and (2) final controlled-aperture migration.

Many wave-equation migration methods make use of reference slownesses during wavefield downward continuation (Stoffa et al., 1990; Huang et al., 1999a, b; Huang and Fehler, 2000b, 2002; Biondi, 2002; Jin et al., 2002). The accuracy of such reference-slowness-based wave-equation migration methods decreases when the migration volume has increasing slowness perturbations. By controlling migration apertures, we can select a reference slowness in controlled regions of the slowness model to reduce slowness perturbations and consequently increase migration accuracy.

The reference-slowness-based wave-equation migration methods are carried out in the dual-domain (the frequency-space and frequency-wavenumber domains). For controlled-aperture migration, the wavefield-downward-continuation computations in the space domain are needed to be performed only within controlled regions, resulting in greater computational efficiency compared to the corresponding uncontrolled-aperture wave-equation migration.

The shapes of the controlled migration apertures do not vary greatly from shot to shot. Therefore, we can use wave-equation migration to determine the controlled migration apertures for only a small subset of shots. We can then use an interpolation scheme to obtain the controlled migration apertures for the other shots. This will significantly reduce the computation cost for migration aperture scan. In addition, we can also reduce the frequency range or increase the frequency interval during migration aperture scan. This will further reduce the computation cost for determining migration apertures.

We will use the synthetic common-shot dataset generated by O'Brien and Gray (1996) with a full-wave-equation finite-difference scheme for a 2D slice of the SEG/EAGE salt model (Aminzadeh et al., 1996) to demonstrate controlled-aperture wave-equation migration. In this paper, we will concentrate our effort on showing the accuracy improvement of controlled-aperture wave-equation migration. We will use controlled-aperture split-step Fourier migration to verify this. The same accuracy improvement can be achieved for the other wave-equation migration methods that use reference slownesses during wavefield downward continuation. Our preliminary numerical tests indicate that the controlled-aperture split-step Fourier migration including migration-aperture scan takes approximately 20% additional computational time compared to the conventional uncontrolled-aperture split-step Fourier migration if we calculate migration apertures using every other frequency component for every other shot.

Migration aperture scan

We used a common-shot dataset for a 2D slice of the SEG/EAGE salt model (Aminzadeh et al., 1996) shown in Figure 1 to illustrate the determination of controlled migration aperture. The dataset was generated by O'Brien and Gray (1996) using a full-wave-equation finite-difference scheme. It

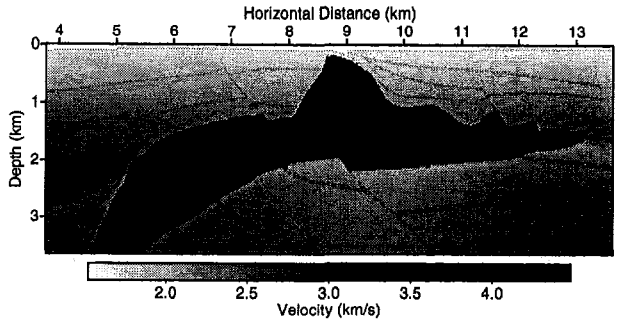

FIG. 1. A 2D slice of the SEG/EAGE salt model. The salt body is shown in black.

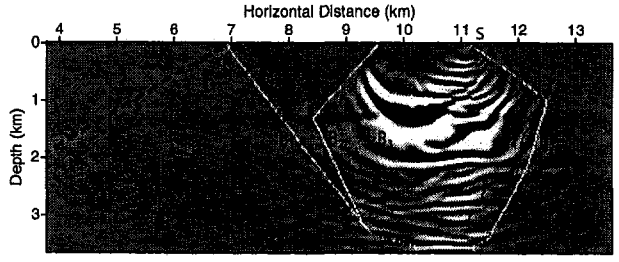

(a) Controlled migration apertures for shot 230

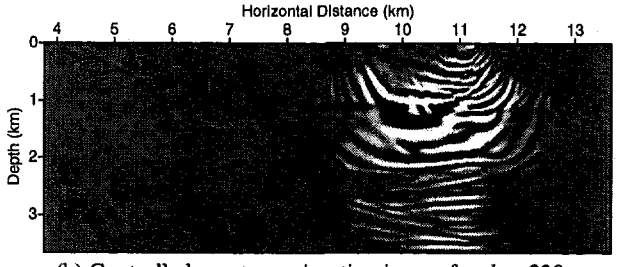

(b) Controlled-aperture migration image for shot 230

FIG. 2. (a) Controlled migration apertures used for shot 230. "S" is the source location and "R" is the receiver location at the maximum offset. The region between two dashed-lines are used to calculate reference slownesses during conventional split-step Fourier migration. (b) Controlled-aperture split-step Fourier migration image using the common-shot gather for shot 230.

contains 325 common-shot gathers, and each shot-gather consists of 176 receivers with an interval of 24.384 m. The shot interval is twice of the receiver spacing. The model was defined in a grid with both horizontal and vertical grid spacing of 24.384 m. The frequency range used for migration was 2–30 Hz.

Figure 2(a) shows a split-step Fourier migration image using one common-shot gather for shot 230. In uncontrolled-aperture wave-equation migration, a region between the dashed lines in Figure 2(a) is generally used to determine the reference slownesses used during wavefield downward continuation, and the wavefield is downward continued into that region. For the controlled-aperture migration, we used the image for a single-shot gather shown in Figure 2(a) to determine an image region. The image was smoothed before migration aperture scan to avoid some isolated image spots that result from noise or numerical artifacts. We used a value of 1%–2% of the maximum image amplitude as a threshold to determine the boundaries of the image region with significant amplitudes. The region with a threshold value of 1% of the maximum image amplitude is bounded by the smoothed black lines B_3 and B_4 in Figure 2(a). We then automatically determined their simple convexes depicted as white lines B_2 and B_5 in Figure 2(a), respectively. The white line B_1 in Figure 2(a) is the simple convex of B_3 with the starting point from the receiver position "R" with the maximum offset.

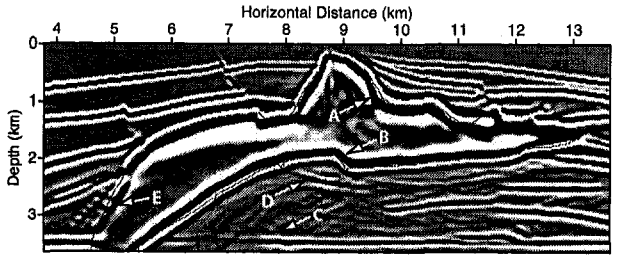

(a) Controlled-aperture split-step Fourier migration

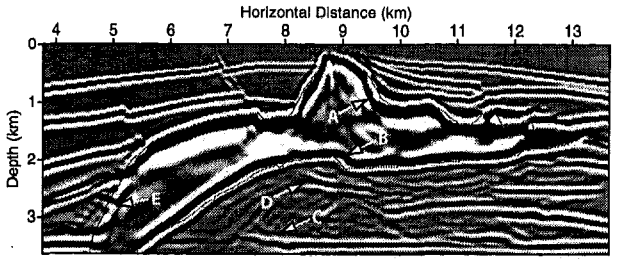

(b) Split-step Fourier migration

FIG. 3. Comparison of the controlled-aperture (a) and uncontrolled-aperture (b) split-step Fourier migration of a common-shot dataset for the 2D salt model shown in Figure 1. The images of the top and bottom of the salt body and those beneath the salt body shown in (a) (such as those locations indicated by "A", "B", "C", "D", and "E") are superior to those in (b). The thin solid lines surrounding the salt body are the correct locations of the top and bottom boundaries of the salt body.

During the final controlled-aperture split-step Fourier migration, we took the Fresnel zone into account and calculated the average slowness within a region whose left and right boundaries are one central wavelength (i.e. the wavelength for the central frequency) inside the region bounded by B_2 and B_5 shown in Figure 2(a), and used it as a reference slowness for downward continuation of the wavefield from the source. Analogously, we calculated the average slowness within a region whose left and right boundaries are one central wavelength inside the region bounded by B_1 and B_5, and used it as a reference slowness for downward continuation of the wavefield from the receivers. The computations of slowness-perturbation correction in the space domain during wavefield downward continuation from the source are needed to be conducted only for a region whose left and right boundaries are one central wave-

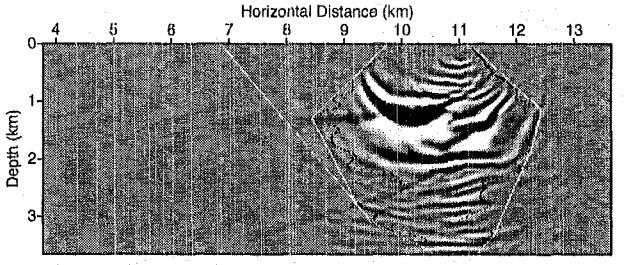

(a) Controlled migration apertures for shot 229

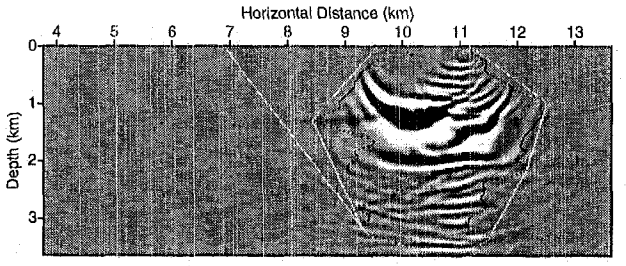

(b) Controlled migration apertures for shot 230

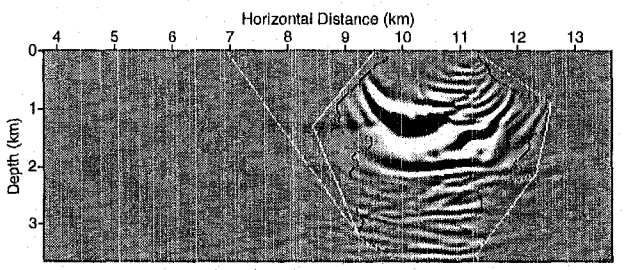

(c) Controlled migration apertures for shot 231

FIG. 4. Comparison of controlled migration apertures used for shot 229 (a), 230 (b), and 231 (c). Migration apertures change gradually rather than dramatically from one shot to its adjacent shots.

length outside the region bounded by B_2 and B_5. During wavefield downward continuation from the receivers, the slowness-perturbation-correction step in the space domain is needed to be carried out only for a region whose left and right boundaries are one central wavelength outside the region bounded by B_1 and B_5. The imaging condition was applied within a region whose left and right boundaries are one central wavelength outside the region bounded by B_3 and B_4. Therefore, the computational time for the final step of controlled-aperture wave-equation migration will be significantly less than the corresponding uncontrolled-aperture wave-equation migration, in which all computations are performed in a region bounded by the dashed lines shown in Figure 2(a).

Figure 2(b) is the controlled-aperture split-step Fourier migration for a common-shot gather of shot 230.

Controlled-aperture migration

Figure 3(a) is the image obtained using the controlled-aperture split-step Fourier migration for the synthetic common-shot dataset for the 2D slice of the SEG/EAGE salt model depicted in Figure 1. Migration aperture scans for all shots were conducted using the split-step Fourier migration scheme. Compared to the corresponding uncontrolled-aperture migration result displayed in Figure 3(b), the controlled-aperture migration image in Figure 3(a) gives more accurate images of the top and bottom of the salt body and of reflectors beneath the salt body. For instance, the image of the interface around location "C" in Figure 3(a) is flat and continuous, but that in Figure 3(b) is discontinuous. In addition, the subsalt reflector image labeled by "D" in Figure 3(a) extends more towards the base salt than that in Figure 3(b).

Figure 4 shows a comparison of migration apertures obtained using the split-step Fourier migration scheme for shots 229, 230, and 231. The shapes of these migration apertures do not change significantly from one shot to its adjacent shots.

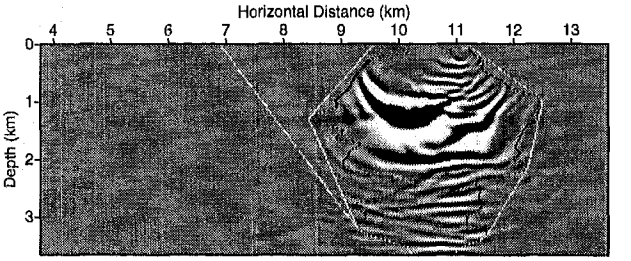

FIG. 5. Migration apertures for shot 230 obtained using every other frequency component.

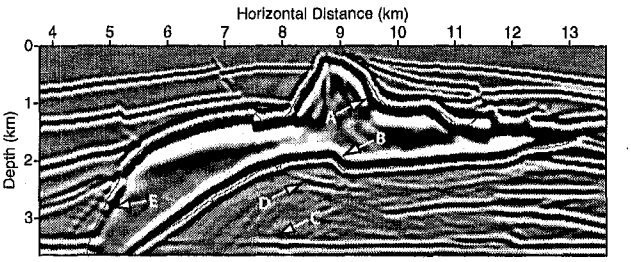

(a)

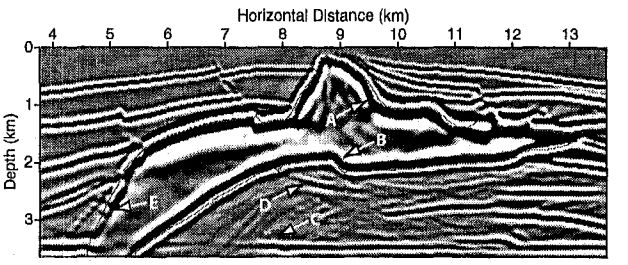

(b)

FIG. 6. Comparison of controlled-aperture migration images of a synthetic common-shot dataset for the 2D salt model shown in Figure 1. (a) is an image obtained using migration apertures calculated by the split-step Fourier method for every other shot. (b) is an image obtained using migration apertures calculated by the split-step Fourier method for every other shot using every other frequency component.

Therefore, we can determine migration apertures for a coarse suite of shots using a wave-equation migration scheme, then interpolate migration apertures for the other shots. This can significantly reduce computational time for migration aperture scan. Furthermore, we can increase the frequency interval used during migration aperture scan to save more computational time. Figure 5 shows migration apertures for shot 230 obtained using every other frequency component. The shapes of the migration apertures in Figure 5 are very similar to those in Figure 4(b) in which all frequency components were used.

The controlled-aperture split-step Fourier migration image obtained using apertures calculated only for odd shots using all frequency components is depicted in Figure 6(a), and that obtained using migration apertures calculated only for odd shots using every other frequency component is displayed in Figure 6(b). All frequency components were used during the final controlled-aperture migrations (the same as Figure 3). We can see that the image quality of Figures 6(a), (b), and Figure 3(a) is very similar. The computational time for obtaining the image in Figure 6(b) was approximately 20% more than that for the conventional uncontrolled-aperture migration producing the image in Figure 3(b). The computation cost for a controlled-aperture split-step Fourier migration can be further reduced by calculating migration apertures for fewer numbers of shots using a wave-equation migration scheme. Further studies are needed to find the maximum shot spacing that can be used for determining migration apertures. A carefully designed controlled-aperture wave-equation migration using common-shot gathers could be up to 50% more efficient than the corresponding uncontrolled-aperture migration for 3D imaging problems.

Conclusions

We have proposed a controlled-aperture wave-equation migration scheme in which migration apertures are determined using a wave-equation migration approach. We have demonstrated that the controlled-aperture migration can improve the accuracy of wave-equation migration methods that use reference slownesses during wavefield downward continuation. We can use the efficient split-step Fourier approach for migration aperture scan, then use other, more accurate though more expensive, wave-equation migration methods such as the globally optimized Fourier finite-difference migration scheme (Huang and Fehler, 2000a) to perform the final controlled-aperture migration. Such a controlled-aperture wave-equation migration could be even more efficient than the uncontrolled-aperture wave-equation migration, while producing more accurate images. Ultimately, a controlled-aperture amplitude-preserving wave-equation migration is required for producing high-quality and reliable images of complex structures.

Acknowledgment

This work was supported by the U.S. Department of Energy through contract W-7405-ENG-36 to Los Alamos National Laboratory.

References

Aminzadeh, F., Burkhard, N., Long, J., Kunz, T., and Duclos, P., 1996, Three dimensional SEG/EAEG models — an update: The Leading Edge, **15**, No. 2, 131–134.

Biondi, B., 2002, Stable wide-angle fourier finite-difference downward extrapolation of 3-D wavefields: Geophysics, **67**, 872–882.

Fehler, M., and Huang, L., 2002, Modern imaging using seismic reflection data: Ann. Rev. Earth. Planet. Sci., **30**, 259–284.

Huang, L., and Fehler, M. C., 2000a, Globally optimized Fourier finite-difference migration method: 70th Ann. Internat. Mtg., Soc. Expl. Geophys., Expanded Abstracts, 802–805.

Huang, L., and Fehler, M. C. 2000b, Quasi-Born Fourier migration: Geophys. J. Intern., **140**, 521–534.

Huang, L., and Fehler, M. C., 2002, Split-step Fourier Padé migration: 72nd Ann. Internat. Mtg., Soc. Expl. Geophys., Expanded Abstracts, 1144–1147.

Huang, L., Fehler, M. C., Roberts, P. M., and Burch, C. C., 1999a, Extended local Rytov Fourier migration method: Geophysics, **64**, 1535–1545.

Huang, L., Fehler, M. C., and Wu, R. 1999b, Extended local Born Fourier migration method: Geophysics, **64**, 1524–1534.

Jin, S., Mosher, C., and Wu, R.-S., 2002, Offset-domain pseudoscreen prestack depth migration: Geophysics, **67**, 1895–1902.

Nemeth, T., Wu, C., and Schuster, G. T., 1999, Least-squares migration of incomplete reflection data: Geophysics, **64**, 208–221.

O'Brien, M. J., and Gray, A. H., 1996, Can we image beneath salt?: The Leading Edge, **15**, No. 1, 17–22.

Stoffa, P. L., Fokkema, J. T., de Luna Freire, R. M., and Kessinger, W. P., 1990, Split-step Fourier migration: Geophysics, **55**, 410–421.

Sun, J., 2000, Limited-aperture migration: Geophysics, **65**, 584–595.